Progress In Electromagnetics Research C, Vol. 124, 167–177, 2022

Sensitivity Estimation of a Planar Optical Waveguide Using Broadband Difference Interferometeric Principle for Detection of Hemoglobin Concentration in Blood

Abhishek Upadhyay[1], Chandan S. Yadav[1], Gulab C. Yadav[1], Shishu P. Singh[2], and Vivek Singh[1, *]

Abstract—Broadband differences interferometeric analysis of a three-layer planar polymer optical waveguide is proposed and optimized to detect the concentration of hemoglobin in blood. The dispersion characteristic and cutoff film thickness of proposed waveguide are obtained by matching the field at various boundaries. The obtained cutoff film thickness for TE_0 and TM_0 modes is 0.09 µm, 0.1 µm at operating wavelength 400 nm, and 0.19 µm and 0.23 µm at operating wavelength 800 nm, respectively. The effective refractive indices of TE_0 and TM_0 modes are obtained at two considered wavelengths, i.e., 400 nm and 800 nm, and hence the difference of their propagation constant is calculated. It is observed that the propagation constant of these modes decreases with the increase of wavelength. Also, the difference of propagation constant attains its maximum value at certain wavelength and decreases either side of this wavelength. The interference maxima signals at output are considered as sensing signal. The maxima of interference signals, close to the maximum value of propagation constant, are shifted sufficiently with the change in cover refractive index. The maximum sensitivity 3.8 nm/RIU is obtained in the proposed broadband differences interferometeric analysis of waveguide at film thickness 300 nm. Hence, at this film thickness the sensing signal changes by 0.68 nm/g/L of hemoglobin concentration in blood.

1. INTRODUCTION

Growing demand for low cost and efficient devices to diagnose the disease in the healthcare and pharmaceutical industries plays a major role behind the development of optical biosensors [1–4]. In this regard, the hemoglobin (HB) is an important protein of our red blood cell which maintain the oxygen level in the body. The monitoring of HB concentration in blood is an important issue because any decrease in HB concentration may cause various deceases [5]. The property of blood can be described by various optical parameters, and it is observed that its refractive index highly depends on the HB concentration in blood [6]. Therefore, it can be easily monitored using optical biosensors. An optical biosensor consists of a bio-receptor to capture the target analyte and a transducer whose optical properties, such as absorption, reflectance, emission, and interferometeric pattern, is altered in the presence of analyte [7, 8]. There are various popular methods for monitoring the change in optical properties, and some of these methods are surface plasmon resonance (SPR) [9], micro-ring resonators [10, 11], reflectometric interference spectroscopy (RifS) [12], photonic interferometric biosensors [13], and planar waveguide interferometers [9, 14]. Out of these methods, it is suggested that the interferometeric analysis provides larger sensitivity by operating them on single wavelength [15].

Received 26 July 2022, Accepted 29 August 2022, Scheduled 22 September 2022

* Corresponding author: Vivek Singh (viveks@bhu.ac.in).

[1] Department of Physics, Institute of Science, Banaras Hindu University, Varanasi 221005, India. [2] Department of Physics, Faculty of Science, R.K.S. Mahavidyalaya, Siddikpur, Jaunpur, UP, India.

Mach-Zehnder and Young interferometers are two popular double-path interferometers that may be able to detect changes in the effective refractive index of the order of 10^{-8}. But in the case of double path interferometer the monochromatic light propagates through two laterally separated waveguide channels. One is called reference arm and the other called sensing arm, which interfere with each other at receiver end and resulting in their relative phase shift. The monochromatic interferometers suggested above result in phase ambiguity. This phase ambiguity problem can be resolved by using broadband interferometers where a continuous light of selected wavelength range is used [16, 17]. Hence to measure refractive index with great accuracy over a wide spectral range, a broadband Mach-Zehnder interferometer is used as an analytical tool, where some suitable arrangement of sensing and reference waveguides results in sinusoidal TE and TM spectra with substantially different Eigen frequencies. Here the instantaneous de-convolution of multiplexed polarizations provides large spectral shifts with small noise. Based on this technique, portable biosensors are demonstrated by some group of researchers [15, 17]. In this regard, the phase signal of two polarizations over a wide spectral range of wavelength is also measured by broadband Young interferometer [18], and a label-free and multiplexed detection of bio-molecules based on this interferometer is demonstrated by Makarona et al. [19]. Further, the basic drawback of these double-path interferometers is that the interference signal becomes highly sensitive to any misalignment of the path or any mechanical noise (vibrations and shocks) present in the path. This drawback of double-path interferometers can be minimized by considering common-path interferometers in which different modes or modes of different orders propagate along single path [20]. Since in common-path interferometers, the cover refractive index highly affects the phase difference between TE-TM modes [21, 22], in the present communication common-path broadband difference interferometeric principle is used to analyze the optical waveguide based sensor.

However, the polymer optical waveguides draw much attention for the fabrication of optical biosensors due to their potential of economic mass production, simplicity and flexibility of waveguide fabrication methods, and suitability to attach with bio-molecules. There are wide ranges of low-cost optical polymers available that retain excellent optical, chemical, and mechanical properties. Most of these polymers are transparent in 400–2000 nm wavelength range and have broad refractive index range from $n = 1.3$ to 1.7 with approximately low losses, i.e., 0.1 dB/cm.

Therefore, in this communication, common path broadband difference interferometer analysis of a planar polymer optical waveguide for measurement of HB concentration is presented. The proposed planar waveguide consists of polystyrene (PS) as waveguide layer and PMMA (poly methyl methacrylate) as substrate, and distil water/blood works as cover layer. This proposed structure has a high contrast in the refractive index and, consequently, may have high mode sensitivity to changes in the system parameters. The present work is organized as follows. The basic theories and mathematical modeling of common path broadband difference interferometer analysis are presented in Section 2. The obtained results are discussed in Section 3. Finally, the important findings are concluded in Section 4.

2. MATHEMATICAL FORMULATION

The proposed three-layer polymer waveguide structure is shown in Fig. 1, in which a phase difference between TE and TM modes is produced by the waveguide structure. The waveguide consists of a film layer of refractive index n_f, thickness d, and a semi-infinite substrate region and cover region of their respective refractive indices n_s and n_c.

This three-layer waveguide supports only those modes for which the constructive interference occurs between the guided beams, after reflection at the two boundaries [23, 24]. Hence, characteristic equations for TE and TM modes are written from Appendix A as:

$$dh - \arctan\left(\frac{p}{h}\right) - \arctan\left(\frac{q}{h}\right) = m\pi \quad \text{for TE} \tag{1}$$

$$dh - \arctan\left(\frac{p}{h}\frac{n_f}{n_s}\right) - \arctan\left(\frac{q}{h}\frac{n_f}{n_c}\right) = m\pi \quad \text{for TM} \tag{2}$$

where $q^2 = \beta^2 - k^2 n_c^2$, $h^2 = k^2 n_f^2 - \beta^2$, $p^2 = \beta^2 - k^2 n_s^2$ and β is the propagation constant given by $\beta = kN$, with N being the guided mode effective refractive index and $k = \frac{2\pi}{\lambda}$. λ is the wavelength of light, and m is the order of the mode. It is observed that the effective index of a guided mode increases

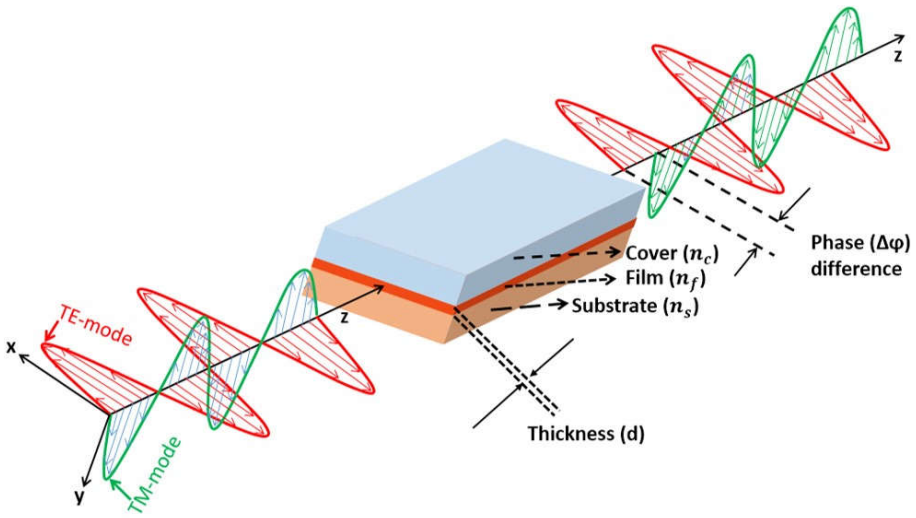

Figure 1. Schematic diagram of proposed three-layer planar waveguide structure.

with film thickness and achieves its maximum value N (free propagation). In this waveguide only those modes propagate for which the film thickness d is greater than the cut-off thickness d_c. Hence the cut-off film thickness d_c is given as [23]

$$d_c(\lambda)\frac{2\pi}{\lambda}\left(n_f^2-n_s^2\right)^{\frac{1}{2}}-\arctan\left[\left(\frac{n_s^2-n_c^2}{n_f^2-n_s^2}\right)^{\frac{1}{2}}\right]=m\pi \quad \text{for TE} \tag{3}$$

$$d_c(\lambda)\frac{2\pi}{\lambda}\left(n_f^2-n_s^2\right)^{\frac{1}{2}}-\arctan\left[\left(\frac{n_f}{n_c}\right)^2\left(\frac{n_s^2-n_c^2}{n_f^2-n_s^2}\right)^{\frac{1}{2}}\right]=m\pi \quad \text{for TM} \tag{4}$$

Since the proposed waveguide is designed to use for sensing application, the cover sensitivity is determined by the change of maxima of output interference signal due to changes of the refractive index of the cover medium Δn_C

$$S\{n_c\}=\frac{\Delta\lambda}{\Delta n_c} \tag{5a}$$

Similarly, the cover sensitivity is also determined by the change of maxima of output interference signal due to the change in HB concentration

$$S\{n_c\}=\frac{\Delta\lambda}{\Delta C} \tag{5b}$$

where ΔC is the change in HB concentration in blood.

The cover region may consist of either pure water or human blood (HB and plasma). The refractive index of HB solution is calculated by using the following equations [6]

$$n_{\mathrm{HB}}=n_{\mathrm{H_2O}}+\alpha C_{\mathrm{HB}} \tag{6}$$

where $n_{\mathrm{H_2O}}=1.3245+\frac{8.4052\times10^3}{\lambda^2}-\frac{3.9572\times10^8}{\lambda^4}-\frac{2.3617\times10^{13}}{\lambda^6}$..., and $\alpha=0.193\times10^{-3}\,\mathrm{L/g}$.

However, modes are the particular pattern of electric field and magnetic field that are repeated as an interval of wavelength. In planar optical waveguides modes are classified as TE_m and TM_m where $m=0$, 1, 2... is the mode order. The phase velocity of mode propagation in optical waveguide is given as $v_f=c/N$, where c is the velocity of light in vacuum. The effective refractive index N depends on polarization, order of mode, wavelength of incident light, refractive index, and thickness of film medium. It also depends on the penetration depth of the evanescent field. The evanescent field is exponentially decreased in the cover medium, hence the penetration depth is given as [25]

$$\Delta z_c=\frac{\lambda}{2\pi}(N^2-n_c)^{-1/2} \tag{7}$$

If the light is coupled into the proposed planar waveguide, then the TE and TM modes are coherently excited. These two modes propagate on a common path and interact with the sample over a length L. After propagating the length L, a phase difference $\Delta\varphi$ between two modes occurs, if the plane of polarization of the output polarizer is set at an angle to the surface of the optical waveguide 45°. The signal recorded by the detector $I(\lambda, t)$ can be expressed by [25, 26]

$$I(\lambda, t) = I_0 \{1 + \cos[\Delta\varphi(\lambda, t)]\} \tag{8}$$

The thickness of film layer is chosen such that only the TE_0 and TM_0 modes of a super-continuum light source propagate in planar waveguide. To obtain the coherence condition of light in waveguide, a polarizer is placed at 45° to the perpendicular direction of the waveguide surface. If $I_0(\lambda)$ is the coupled optical power of the orthogonal modes TE_0 and TM_0, then the spectral signal $I(\lambda)$ is given by

$$I(\lambda) = \frac{1}{2} I_0(\lambda) \{1 + \cos[\Delta\varphi(\lambda)]\} \tag{9}$$

These two orthogonal modes may experience different effective refractive indices over the propagation length L; hence the phase difference between the modes at the output of waveguide is given as

$$\Delta\varphi(\lambda) = \frac{2\pi}{\lambda} L [N_{\mathrm{TM}}(\lambda) - N_{\mathrm{TE}}(\lambda)] \tag{10}$$

The normalized distribution of light intensity at the structure at output is

$$I_n(\lambda) = \{1 + \cos[\Delta\varphi(\lambda)]\} \tag{11}$$

It is clear from Equation (10) that the phase change $\Delta\varphi$ between the modes depends on propagation path length L, effective refractive indices (N_{TM}, N_{TE}), and wavelength λ. The phase change per unit of the propagation path length can be determined by using the mode propagation constant β. Hence, it can be used to describe the phenomena of broadband interference. β is proportional to effective refractive index that is expressed as

$$\beta_i(\lambda, n_c) = \frac{2\pi}{\lambda} N_i(\lambda, n_c) \tag{12}$$

By solving Equations (10), (11), and (12), we have

$$\Delta\phi(\lambda, n_c) = \Delta\beta(\lambda, n_c) \cdot L \tag{13}$$

where $\Delta\beta$ is the difference between the propagation constants of the TE and TM modes.

3. RESULTS AND DISCUSSION

In order to analyze polymer waveguide based broadband difference interferometer, a three-layer planar waveguide is considered. The waveguide has a film layer of polystyrene (PS) which is sandwiched between a semi-infinite substrate layer of poly methyl methacrylate (PMMA) and a semi-infinite cover layer of either pure water or HB solution. Using Equations (1) and (2), dispersion curve of the proposed waveguide is plotted and shown in Figs. 2(a) and 2(b) for TM modes and TE modes, respectively. The effective refractive indices of proposed waveguide at the shortest 400 nm and longest 800 nm wavelengths of light are calculated as a function of the film thickness d from minimum deviation prism method [27]. It is clear from Fig. 2 that the TE_0 and TM_0 modes at wavelength 400 nm have respective cutoff film thicknesses 0.09 μm and 0.11 μm, and at 800 nm wavelength the cutoff film thicknesses are 0.19 μm and 0.23 μm. These cutoff values of film thicknesses (d_c) can also be calculated by using Equations (3) and (4). The dependence of the cut-off film thicknesses of the modes on the incident wavelength is plotted in Fig. 3.

This curve is plotted to select the film layer thickness and respective wavelength for which only the propagation of TE_0 and TM_0 modes is possible. For further analysis of the proposed waveguide, the film thicknesses $d_1 = 300$ nm, $d_2 = 350$ nm, $d_3 = 400$ nm, $d_4 = 450$ nm, and $d_5 = 500$ nm are selected. It is clear from Fig. 3 that the film thicknesses $d_4 = 450$ nm and $d_5 = 500$ nm are not single mode in the considered wavelength range. These selected film thicknesses are marked with red arrow lines in Fig. 2 that reflects the ranges of change in the effective refractive index for both TE_0 and TM_0 polarizations.

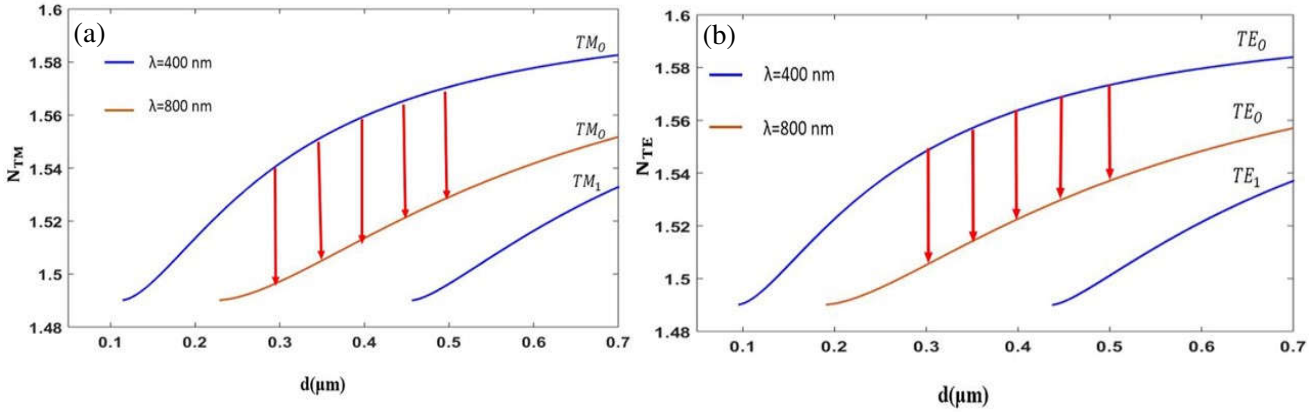

Figure 2. Variation of effective refractive indices for as a function of the film layer thickness d for (a) TM mode, (b) TE mode.

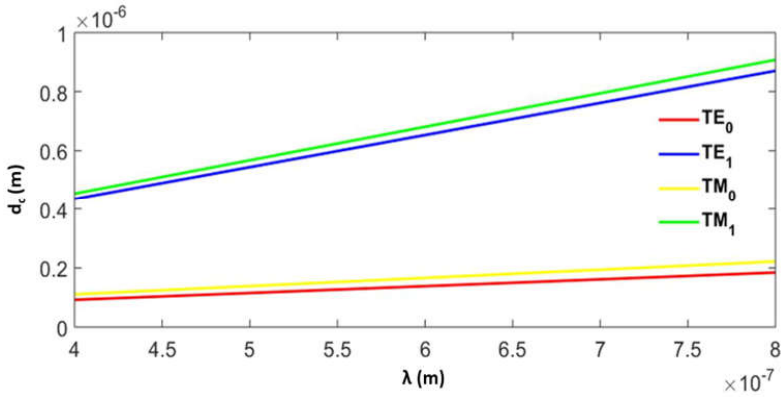

Figure 3. Variation of the cutoff film thickness with wavelength for first two lower order modes.

Using Equation (12) the propagation constants for TM mode are calculated, and their variation with wavelength is plotted at fixed film thickness as shown in Fig. 4(a). The similar exercise has been done of TE modes and is shown in Fig. 4(b). It is found that the propagation constant monotonically decreases for both TE_0 and TM_0 propagating modes in considered wavelength range. It is also observed that larger values of propagation constant are observed for larger film thickness at fixed wavelength.

Further, the difference of TE_0 and TM_0 propagation constants, i.e., $\Delta\beta(\lambda, n_c)$ as a function of the wavelength at considered film thicknesses is plotted as shown in Fig. 5, and hence phase difference dependence $\Delta\varphi(\lambda, n_c)$ is calculated using Equation (10). It is clear from this figure that at film thickness of 300 nm, 350 nm, and 400 nm, $\Delta\beta(\lambda, n_c)$ first increases up to their respective maximum value 0.01683 μm^{-1}, 0.01446 μm^{-1}, and 0.01265 μm^{-1}, and then starts decreasing under considered wavelength range. This maximum value of $\Delta\beta$ is red shifted with the increase of film thickness. Other two considered thickness (450 nm and 500 nm) difference of propagation constants increases with the increase in the wavelength in considered wavelength range. Since 300 nm thick film layer of waveguide shows maximum change in propagation constant, this thickness is selected to observe the impact of cover refractive index on the output signal.

The variation in $\Delta\beta$ with wavelength, after passing to a 1 mm propagation path in the proposed three-layer waveguide having pure water (n_{c1}) in cover region is plotted and shown by the blue continuous line in Fig. 6. The blue dotted line in this figure shows the variation in $\Delta\beta$ with wavelength after increasing the cover refractive index by 0.001 (n_{c2}). Here a parallel shift in propagation constant difference along the function value axis is observed. The respective phase between modes can be easily determined using Equation (12). Here the obtained phase difference decreases with the increase of cover

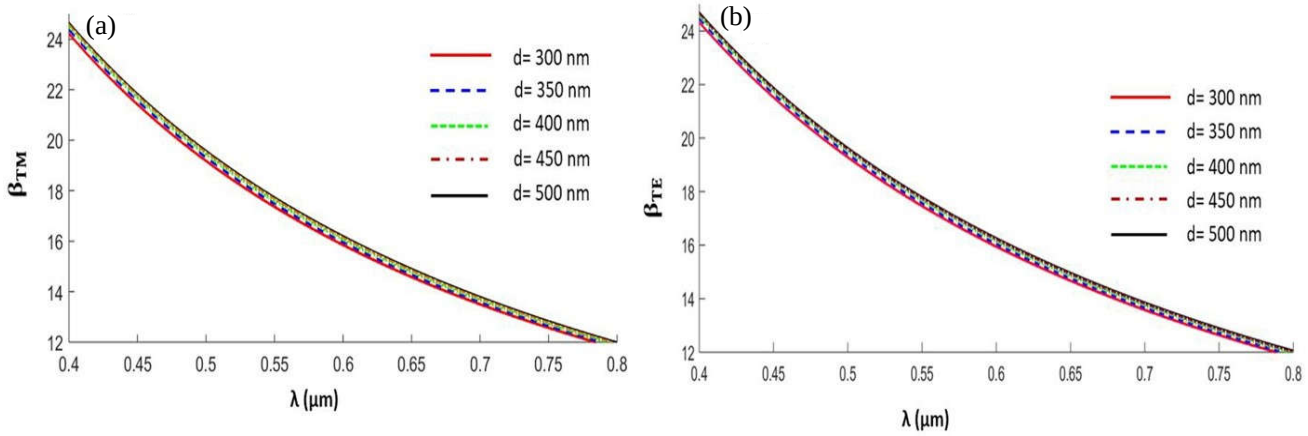

Figure 4. Dependency of propagation constants of proposed waveguide with wavelength at fixed film thickness for (a) TM modes, (b) TE mode.

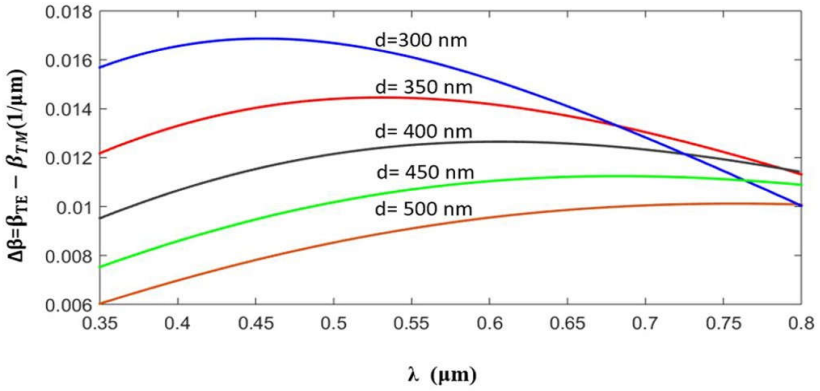

Figure 5. Variation of propagation constants difference with wavelength at fixed film thicknesses.

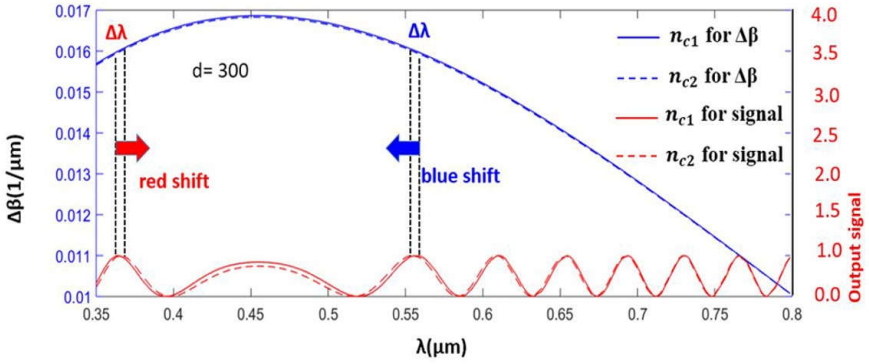

Figure 6. Variation of output interference signal with incident wavelength at 300 nm of film thickness and 1 mm length of propagation path of proposed waveguide having pure water (solid line) in cover region and after increasing cover refractive index by 0.001 (dotted line).

refractive index in all wavelengths in the range under consideration. The output interference signal in the presence of pure water in cover region is also plotted in Fig. 6 and shown by red solid line while after increasing the cover refractive index by 0.001 is plotted by red dotted line. The variation of $\Delta\beta$ and the output signal with wavelength for two above mentioned cover refractive index can also be plotted

at other considered film thicknesses, i.e., 350 nm, 400 nm, 450 nm, and 500 nm. The maximum value of output interference signal occurs when its phase difference is equal to integral multiple of 2π. Since in this study a continuous source of light (400 nm to 800 nm) is used, at zero phase difference region (near the maximum value of $\Delta\beta$) the interference signals have the same value for each wavelength, hence a wider interference signal is obtained. If the refractive index of sensing region changes, i.e., the cover refractive index changes, which changes the phase shift, as a consequence of this the output interference signal of the system will change. This change in output interference signal is prominent close to the wavelength range where $\Delta\beta$ has its maximum value. This effect can be visualized by considering the maxima of the output interference signal. The maxima of the output signals are marked on both sides near the maximum value of $\Delta\beta$ curve by black dotted line as shown in Fig. 6. Here, by changing the cover refractive index the selected maximum is shifted towards the longer wavelength, i.e., red shifted when phase shift $\Delta\varphi$ increases with wavelength and the other selected maximum is shifted towards the shorter wavelength, i.e., blue shifted when phase shift $\Delta\varphi$ decreases with wavelength. Around the maximum value of $\Delta\beta$, this phase change is constant with wavelength, but its value depends on cover refractive index. It is also clear from Fig. 6 that the distance between two successive maxima of output interference signal is larger near the change of slope of the phase difference. Further, the mode sensitivities due to change in cover refractive index of proposed waveguide at film thickness $d = 300$, 350, 400, 450 and $d = 500$ nm are calculated. The obtained sensitivities at respective film thicknesses are 3.8 nm/RIU, 3.6 nm/RIU, 3.5 nm/RIU, 1.8 nm/RIU, and 1.6 nm/RIU. It is clear that the sensitivity of proposed waveguide decreases with the increase of film thickness, and maximum sensitivity is observed at 300 nm of film thickness for our considered cases.

Hence, this film thickness is used to find the variation of $\Delta\beta$ and the output signal with wavelength at different HB concentration as shown in Fig. 7. In this figure the variation of HB concentration lies between 40 and 160 g/L with 40 g/L increment. It is clear from the output interference signal that the output interference signal, the maxima shifted with increment of the HB concentration. The HB concentration sensitivity of proposed sensor at various concentrations is calculated and tabulated in Table 1. It is clear from Table 1 that the sensitivity decreases with the increase of HB concentration. Here the maximum obtained sensitivity for HB concentration is 0.68 nm/(g/L).

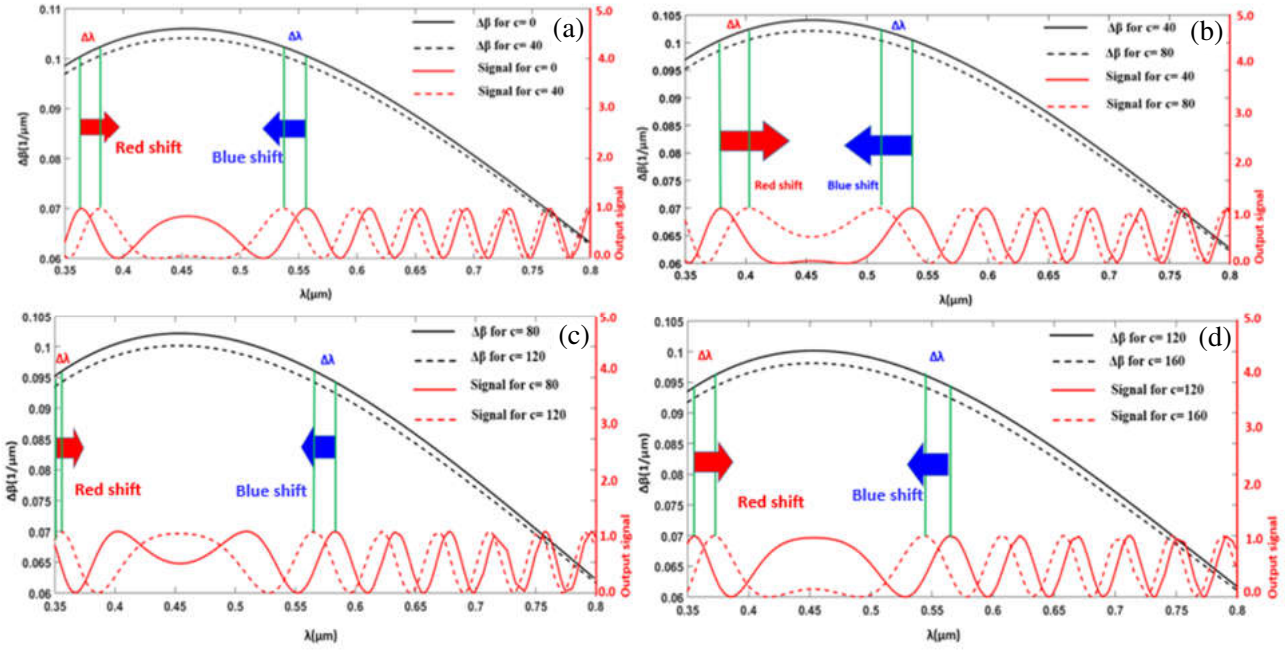

Figure 7. Variations in $\Delta\beta$ (black line) and output signal (red line) with incident wavelength for (a) 0–40 g/L, (b) 40–80 g/L, (c) 80–120 g/L and (d) 120–160 g/L concentration of HB in blood at fixed film layer thicknesses 300 nm and 1 mm propagation length of waveguide.

Table 1. Sensitivity of proposed sensor for each 40 (g/L) increment of HB concentration.

HB concentration C/(g/L)	Wavelength Shift (nm)	Sensitivity nm/(g/L)
40	17.1	0.43
80	27.0	0.68
120	18.0	0.45
160	19.8	0.49

4. CONCLUSIONS

The sensitivity of a three-layer planar polymer waveguide is optimized utilizing common path broadband difference interferometeric principle and demonstrated for the detection of HB concentration in blood. The proposed waveguide is analyzed by considering the film thicknesses 300 nm, 350 nm, 400 nm, 450 nm, and 500 nm in which the film thicknesses 450 nm and 500 nm do not lie in the single mode waveguide within the considered wavelength range 400–800 nm. The propagation constant difference of TE_0 and TM_0 modes at two considered wavelengths, i.e., 400 nm and 800 nm, is obtained. This propagation constant difference $\Delta\beta$ has its maximum value at 300 nm film thickness in all considered cases. The first maximum of output interference signal close to the maximum of propagation constant difference is considered as a sensing signal that gives maximum shifts compared to the other output interference signal maxima. The shifts of output signal maxima due to change in cover refractive index also depend on the direction of slope of phase difference, i.e., red shifted when phase shift $\Delta\varphi$ increases with wavelength and blue shifted when phase shift $\Delta\varphi$ decreases with wavelength. The optimized waveguide shows maximum sensitivity 3.8 nm/RIU at 300 nm film thickness. The maximum obtained sensitivity of proposed sensor with HB concentration is 0.68 nm/(g/L).

ACKNOWLEDGMENT

Abhishek Upadhyay and Chandan Singh Yadav are thankful to University Grant Commission (Government of India, New Delhi) and DST-INSPIRE (Department of Science and Technology, Government of India, New Delhi) for providing fellowships respectively.

Declarations

Funding Statement:

The authors acknowledge support from the Institutions of Eminence (IoE) Banaras Hindu University Grant scheme No. 6031.

Conflict of Interest:

The authors declare that they have no conflicts of interest.

Author Contributions:

VS conceive the idea. AU, CSY, GCY did simulations. AU, CSY, GCY, SPS and VS discussed and analyzed the results. AU wrote the manuscript. All authors contributed equally for this work.

Availability of Data and Material:

My research didn't generate any data or I reused existing data.

Compliance with Ethical Standards:

This article does not contain any studies involving animals or human participants performed by any of the authors.

Consent to Participate:

Not Applicable.

Consent for Publication:

Not Applicable.

APPENDIX A.

The performance of proposed biosensor is obtained by solving Maxwell's equations for a three-layer structure, and the Helmholtz equations are obtained which can be written as

$$\frac{\partial^2 F(z)}{\partial x^2} + \left(k^2 n^2 - \beta^2\right) F(z) = 0 \tag{A1}$$

where $F = E$ or H depending on the light polarization, and $\beta = k_0 N$, with k_0 being the free space wavenumber and N the model effective index.

The solutions of proposed waveguide for different regions can be written as:

$$F(z) = \begin{cases} A_S e^{-ipz} e^{i(k_x x - \omega t)} & \text{(Substrate)} \\ \left(A_F e^{ihz} + B_F e^{-ihz}\right) e^{i(k_x x - \omega t)} & \text{(Film)} \\ A_C e^{-iqz} e^{i(k_x x - \omega t)} & \text{(Cover)} \end{cases} \tag{A2}$$

where $q^2 = \beta^2 - k^2 n_c^2$, $h^2 = k^2 n_f^2 - \beta^2$, $p^2 = \beta^2 - k^2 n_s^2$.

Here, n_c, n_f, and n_s are refractive indices of cover, film, and substrate region, respectively.

By matching the fields and applying the following boundary conditions:

(i) For TE mode, F and $\frac{\partial F}{\partial z}$ are continuous across the two boundaries.

(ii) For TM mode, F and $\left(\frac{1}{n^2}\right)\frac{\partial F}{\partial z}$ are continuous across the two boundaries.

By using above boundary conditions, the matrix equation can be written in the following form:

$$A_\rho \xi = 0. \tag{A3}$$

where, $\boldsymbol{\xi} = \begin{pmatrix} A_s \\ A_F \\ B_F \\ A_c \end{pmatrix}$ and $\mathbf{A}_\rho = \begin{pmatrix} 1 & -1 & -1 & 0 \\ 0 & -e^{ihd_f} & -e^{-ihd_f} & e^{-iqd_f} \\ \frac{p}{n_s^{2\rho}} & \frac{h}{n_f^{2\rho}} & -\frac{h}{n_f^{2\rho}} & 0 \\ 0 & -\frac{h}{n_f^{2\rho}} e^{ihd_f} & \frac{h}{n_f^{2\rho}} e^{-ihd_f} & \frac{h}{n_f^{2\rho}} e^{ihd_f} \end{pmatrix}$.

The above equation can be written for TE modes by putting $\rho = 0$ and for TM modes $\rho = 1$.

It is clear from above equation that the coefficient matrix $\xi \neq 0$, so to get nontrivial solution

$$|A_\rho| = 0 \tag{A4}$$

A waveguide mode arises when the reflected beams in the film achieve constructive interference upon experiencing reflections. The constructive interference between the guided beams exists if the wave fronts are in phase after reflection at the two boundaries i.e., the total phase shift should be an integral multiple of 2π. So, by solving above Eq. (A4) the dispersion relation for the proposed waveguide can be written as:

$$dh - \arctan\left(\frac{p}{h}\right) - \arctan\left(\frac{q}{h}\right) = m\pi \quad \text{for TE mode} \tag{A5}$$

$$dh - \arctan\left(\frac{p}{h}\frac{n_f}{n_s}\right) - \arctan\left(\frac{q}{h}\frac{n_f}{n_c}\right) = m\pi \quad \text{for TM mode} \tag{A6}$$

where $m = 0, 1, 2...$ is the order of mode.

Above proposed waveguide supports only those modes for which the film thickness d is greater than the cut-off thickness d_c. Hence for cut-off film thickness d_c, Eqs. (A5) & (A6) can be modified by putting $h,\ p$, and q expressions from Eq. (A2);

$$d_c\left(\lambda\right)\frac{2\pi}{\lambda}\left(n_f^2-n_s^2\right)^{\frac{1}{2}}-\arctan\left[\left(\frac{n_s^2-n_c^2}{n_f^2-n_s^2}\right)^{\frac{1}{2}}\right]=m\pi\quad\text{for TE} \tag{A7}$$

$$d_c\left(\lambda\right)\frac{2\pi}{\lambda}\left(n_f^2-n_s^2\right)^{\frac{1}{2}}-\arctan\left[\left(\frac{n_f}{n_c}\right)^2\left(\frac{n_s^2-n_c^2}{n_f^2-n_s^2}\right)^{\frac{1}{2}}\right]=m\pi\quad\text{for TM} \tag{A8}$$

REFERENCES

1. Du, H., Z. Li, Y. Wang, Q. Yang, and W. Wu, "Nanomaterial-based optical biosensors for the detection of foodborne bacteria," *Food Reviews International*, Vol. 38, No. 4, 655–684, 2020, doi: 10.1080/87559129.2020.1740733.
2. Singh, V. and D. Kumar, "Theoretical modeling of a metal-clad planar waveguide based biosensors for the detection of pseudomonas-like bacteria," *Progress In Electromagnetics Research M*, Vol. 6, 167–184, 2009.
3. Samson, R., G. R. Navale, and M. S. Dharne, "Biosensors: Frontiers in rapid detection of COVID-19," *3 Biotech*, Vol. 10, No. 385, 1–9, 2020, doi: 10.1007/S13205-020-02369-0.
4. Liu, N., S. Wang, J. Wang, J. Lv, Q. Cheng, W. Ma, and Y. Lu, "Dual-band reflective optical sensor based on GMR-TPS structure to detect the hemoglobin," *IEEE Sensors Journal*, Vol. 22, No. 13, 13529–13535, 2022, doi: 10.1109/JSEN.2022.3179010.
5. Beutler, E. and J. Waalen, "The definition of anemia: What is the lower limit of normal of the blood hemoglobin concentration?," *Blood*, Vol. 107, 1747–1750, 2006, doi: 10.1182/BLOOD-2005-07-3046.
6. Friebel, M. and M. Meinke, "Model function to calculate the refractive index of native hemoglobin in the wavelength range of 250–1100 nm dependent on concentration," *Applied Optics*, Vol. 45, No. 12, 2838–2842, 2006, doi: 10.1364/AO.45.002838.
7. Peltomaa, R., B. Glahn-Martínez, E. Benito-Peña, and M. C. Moreno-Bondi, "Optical biosensors for label-free detection of small molecules," *Sensors*, Vol. 18, No. 4126, 1–46, 2018, doi: 10.3390/S18124126.
8. Liu, X., Y. Gu, C. Huang, M. Zhao, Y. Cheng, E. G. A. Jawdeh, H. S. Bada, L. Chen, and G. Yu, "Simultaneous measurements of tissue blood flow and oxygenation using a wearable fiber-free optical sensor," *J. of Biomedical Optics*, Vol. 26, No. 1, 012705, 2021, doi: 10.1117/1.JBO.1.012705.
9. Goodrich, T. T., H. J. Lee, and R. M. Corn, "Direct detection of genomic DNA by enzymatically amplified SPR imaging measurements of RNA microarrays," *J. Am. Chem. Soc.*, Vol. 126, 4086–4087, 2004, doi: 10.1021/ja039823p.
10. Bahadoran, M., A. K. Seyfari, P. Sanati, and L. S. Chua, "Label free identification of the different status of anemia disease using optimized double-slot cascaded microring resonator," *Scientific Reports*, Vol. 12, No. 5548, 2022, doi: 10.1038/s41598-022-09504-2.
11. Kitsara, M., K. Misiakos, I. Raptis, and E. Makarona, "Integrated optical frequency-resolved Mach-Zehnder interferometers for label-free affinity sensing," *Optics Express*, Vol. 18, 8193, 2010, doi: 10.1364/oe.18.008193.
12. Lu, J., C. M. Strohsahl, B. L. Miller, and L. J. Rothberg, "Reflective interferometric detection of label-free oligonucleotides," *Analytical Chemistry*, Vol. 76, 4416–4420, 2004, doi: 10.1021/ac0499165.
13. Calo, G., A. Farinola, and V. Petruzzelli, "Design and optimization of high sensitivity photonic interferometric biosensors on polymeric waveguides," *Progress In Electromagnetics Research Letters*, Vol. 33, 151–166, 2012.

14. Kozma, P., F. Kehl, E. Ehrentreich-Förster, C. Stamm, and F. F. Bier, "Integrated planar optical waveguide interferometer biosensors: A comparative review," *Biosensors and Bioelectronics*, Vol. 58, 287–307, 2014, doi: 10.1016/j.bios.2014.02.049.
15. Xie, Y., M. Zhang, and D. Dai, "Design rule of Mach-Zehnder interferometer sensors for ultra-high sensitivity," *Sensors (Switzerland)*, Vol. 20, 1–8, 2020, doi: 10.3390/s20092640.
16. Wang, F., S. Ma, T. Ma, X. Wang, K. Yu, and L. Li, "Refractive index sensing performances of a mid-infrared asymmetric MZI based on suspended GaAs waveguides," *Progress In Electromagnetics Research M*, Vol. 111, 173–183, 2022.
17. Casquel, R., M. Holgado, M. F. Laguna, A. L. Hernández, B. Santamaría, Á. Lavín, L. Tramarin, and P. Herreros, "Engineering vertically interrogated interferometric sensors for optical label-free biosensing," *Analytical and Bioanalytical Chemistry*, Vol. 412, 3285–3297, 2020, doi: 10.1007/S00216-020-02411-3.
18. Savra, E., A. Malainou, A. Salapatas, A. Botsialas, P. Petrou, I. Raptis, E. Makarona, S. E. Kakabakos, and K. Misiakos, "Monolithically-integrated Young interferometers for label-free and multiplexed detection of biomolecules," *Silicon Photonics XI*, Vol. 9752, 97520N, 2016, doi: 10.1117/12.2209011.
19. Makarona, E., A. Salapatas, I. Raptis, P. Petrou, S. Kakabakos, E. Stavra, A. Malainou, and K. Misiakos, "Broadband Young interferometry for simultaneous dual polarization bioanalytics," *J. Opt. Soc. Am. B*, Vol. 34, 1691, 2017, doi: 10.1364/josab.34.001691.
20. Dyson, J., "Very stable common-path interferometers and applications," *J. Opt. Soc. Am.*, Vol. 53, 690, 1963, doi: 10.1364/josa.53.000690.
21. Stamm, C. and W. Lukosz, "Integrated optical difference interferometer as immunosensor," *Sensors and Actuators B: Chemical*, Vol. 31, 203–207, 1996, doi: 10.1016/0925-4005(96)80067-0.
22. Tyszkiewicz, C., T. Pustelny, and T. Pustelny, "Differential interferometry in planar waveguide structures with ferronematic layer Special Issue "Design and Application of Modern Evanescent Wave Photonic Sensors" in special the issue of Photonics (ISSN 2304-6732) View project maciej.setkiewicz@polsl.pl View project 56 PUBLICATIONS 307 CITATIONS SEE PROFILE Differential interferometry in planar waveguide structures with ferronematic layer," *Optica Applicata*, Vol. XXXIV, 2004.
23. Boudrioua, A., "Photonic waveguides: Theory and applications," *Photonic Waveguides: Theory and Applications*, Wiley-ISTE, 2009, doi: 10.1002/9780470611142.
24. El-Agez, T. and S. Taya, "Theoretical spectroscopic scan of the sensitivity of asymmetric slab waveguide sensors," *Optica Applicata*, Vol. 41, 90–95, 2011.
25. Lukosz, W. and C. Stamm, "Integrated optical interferometer as relative humidity sensor and differential refractometer," *Sensors and Actuators A: Physical*, Vol. 25, 185–188, 1990, doi: 10.1016/0924-4247(90)87029-I.
26. Stamm, C. and W. Lukosz, "Integrated optical difference interferometer as refractometer and chemical sensor," *Sensors and Actuators B: Chemical*, Vol. 11, 177–181, 1993, doi: 10.1016/0925-4005(93)85252-6.
27. Daimon, M. and A. Masumura, "Measurement of the refractive index of distilled water from the near-infrared region to the ultraviolet region," *Applied Optics*, Vol. 46, 3811–3820, 2007, doi: 10.1364/AO.46.003811.